African burned area and fire carbon emissions are strongly impacted by small fires undetected by coarse resolution satellite data

Ruben Ramo[a,b,1], Ekhi Roteta[c], Ioannis Bistinas[d,e], Dave van Wees[d], Aitor Bastarrika[c], Emilio Chuvieco[b], and Guido R. van der Werf[d]

[a]COMPLUTIG–Complutum Tecnologías de la Información Geográfica SL, 28801 Alcalá de Henares, Spain; [b]Environmental Remote Sensing Research Group, Department of Geology, Geography and the Environment, University of Alcalá, 28801 Alcalá de Henares, Spain; [c]Department of Mining and Metallurgical Engineering and Materials Science, School of Engineering of Vitoria-Gasteiz, University of the Basque Country, 01006 Vitoria-Gasteiz, Spain; [d]Faculty of Science, Vrije Universiteit, 1081HV Amsterdam, The Netherlands; and [e]Atos Nederland B.V. Burg, 1185MC Amstelveen, The Netherlands

Edited by Karen C. Seto, Yale University, New Haven, CT, and approved December 29, 2020 (received for review June 10, 2020)

Fires are a major contributor to atmospheric budgets of greenhouse gases and aerosols, affect soils and vegetation properties, and are a key driver of land use change. Since the 1990s, global burned area (BA) estimates based on satellite observations have provided critical insights into patterns and trends of fire occurrence. However, these global BA products are based on coarse spatial-resolution sensors, which are unsuitable for detecting small fires that burn only a fraction of a satellite pixel. We estimated the relevance of those small fires by comparing a BA product generated from Sentinel-2 MSI (Multispectral Instrument) images (20-m spatial resolution) with a widely used global BA product based on Moderate Resolution Imaging Spectroradiometer (MODIS) images (500 m) focusing on sub-Saharan Africa. For the year 2016, we detected 80% more BA with Sentinel-2 images than with the MODIS product. This difference was predominately related to small fires: we observed that 2.02 Mkm^2 (out of a total of 4.89 Mkm^2) was burned by fires smaller than 100 ha, whereas the MODIS product only detected 0.13 million km^2 BA in that fire-size class. This increase in BA subsequently resulted in increased estimates of fire emissions; we computed 31 to 101% more fire carbon emissions than current estimates based on MODIS products. We conclude that small fires are a critical driver of BA in sub-Saharan Africa and that including those small fires in emission estimates raises the contribution of biomass burning to global burdens of (greenhouse) gases and aerosols.

Sentinel 2 | Africa | MODIS | small fires | carbon emissions

Fire plays an important role in the Earth system, impacting climate and air quality and affecting vegetation, soils, and human assets (1–3). Global annual BA is currently estimated to be between 4.2 and 4.7 million km^2 (4–6). Fires burn naturally in many ecosystems, but currently, the majority of fires have an anthropogenic origin and are often used as a land management tool [e.g., in the deforestation process (4, 5)]. Fires impact climate by releasing greenhouse gases and aerosols and by modifying surface albedo (6–8).

Satellite sensors are the preferred way to estimate BA, as they provide frequent and comprehensive observations of surface reflectance and thermal properties (9). However, most existing products are based on coarse spatial-resolution images (≥500 m), which provide a global view of fire occurrence almost daily but may have important omission and commission errors, particularly where fires are small in size (10). In fact, several regional assessments of those global BA products have identified substantial omission errors when compared to fire perimeters (11–15). Omission of small fires may be the cause of observing higher omission than commission errors in existing validation efforts of global BA products (15–17).

A first approach to estimate the contribution of these small fires was proposed by Randerson et al. (18) based on a statistical method overlaying BA and active fire detections. They estimated that small fires led to an additional 24 to 54% BA compared to previous estimates. Thanks to recent developments in satellite instruments and computing power, we can now map BA with substantially higher spatial resolution (≤30 m) and for large geographic regions (19–21), reducing the dependency on statistical methods and active fire detections.

Our main goal was to compare a new BA dataset generated from medium-resolution images and its resulting fire carbon emissions with existing information based on global BA datasets derived from coarse-resolution data. We focused our analysis on Africa, as it accounts for about 70% of global BA (22) and about half of global fire carbon emissions (23). The medium-resolution BA product was developed from Sentinel-2 MultiSpectral Instrument (MSI) data under the Fire Disturbance project of the European Space Agency's Climate Change Initiative (CCI) program. The product, named FireCCISFD11, covers the whole of sub-Saharan Africa at 20-m resolution for the year 2016 (21) (see *Materials and Methods*). We have compared this product with three global BA datasets derived from MODIS data: MCD64A1C6 (22), the Global Fire Emission Database version 4s (GFED4s) (23), and the Global Fire Atlas (GFA) (24). MCD64A1C6 is the most recent version of a widely used BA product for global analysis of biomass burning impacts (9, 25). GFED4s is based on an older version of the MCD64A1 dataset (C5.1) but includes BA estimates from small fires based on a

Significance

Fires burn an area comparable to Europe each year, emitting greenhouse gases and aerosols. We compared burned area (BA) based on 20-m resolution images with a BA derived from 500-m data. It represents an 80% increase in BA in sub-Saharan Africa, responsible for about 70% of global BA. This difference is predominately (87%) attributed to small fires (<100 ha), which account for 41% of total BA but only for 5% in coarse-resolution products. We found that African fires were responsible for emissions of 1.44 PgC, 31–101% higher than previous estimates and representing 14% of global CO_2 emissions from fossil fuel burning. We conclude that small fires are critically important in characterizing the most important disturbance agent on a global scale.

Author contributions: R.R., I.B., E.C., and G.R.v.d.W. designed research; R.R., D.v.W., E.C., and G.R.v.d.W. performed research; R.R., E.R., I.B., D.v.W., and A.B. contributed new reagents/analytic tools; R.R., E.R., D.v.W., and G.R.v.d.W. analyzed data; and R.R., E.C., and G.R.v.d.W. wrote the paper.

The authors declare no competing interest.

This article is a PNAS Direct Submission.

[1]To whom correspondence may be addressed. Email: ruben.ramo@uah.es.

Published February 22, 2021.

statistical approach. This product is only available at 0.25° spatial resolution (23). The GFA was derived from the MCD64A1C6 product. It generates burned patches from detected burned pixels using contextual analysis (24). Our comparative analysis between FireCCISFD11 and global products included total BA (with MCD64A1 and GFED4s), fire size distribution (with MCD64A1 and GFA), BA stratified by land cover (MCD64A1), and fire emissions (derived from MCD64A1 and GFED4s).

Revised BA Estimates

The FireCCISFD11 product detected 4.89 Mkm^2 of BA for all of sub-Saharan Africa (representing 16% of the total land area of the region). For the same year and area, this estimate is 80% higher than the BA detected by the MCD64A1C6 product (2.72 Mkm^2) and 63% higher than GFED4s (2.98 Mkm^2). Most BA occurred around the 10°N and 10 to 20°S latitude belts (Fig. 1*A*), which are mostly occupied by savannas. These areas generally receive enough precipitation during the wet season for fuel buildup, while the dry season is long enough to dry out the fuels. No BA was observed in desert areas with little available fuel, and small amounts of BA were found around the Equator where the dry season is short and the vegetation is less susceptible to fire.

While the FireCCISFD11 product had substantially more BA than GFED4s, the general spatial distribution of BA between the products was found to be similar (Fig. 1). The largest differences between the two products were observed in the Northern Hemisphere in Kenya (203% more BA), Cameroon (+122%), Guinea-Bissau (+117%), and Nigeria (+83%) and in the Southern Hemisphere in Malawi (+255%), South Africa (+177%), Tanzania (+104%), and Madagascar (+199%). In terms of land cover, as defined by the classes of the S2 Land cover Map for Africa with 20-m spatial resolution (26), the largest increase was observed in shrublands (173% more BA), forests (+163%), grasslands (+191%), and croplands (+270%). In some areas of Sudan and Congo, GFED4s showed more BA than FireCCISFD11, mostly due to a smaller sample of valid observations from the Sentinel-2 MSI sensor compared to the MODIS BA products as well as the longer revisit times of MSI over MODIS sensors (10 versus 1 d).

Fire-Size Distribution: Relevance of Small Fires

Fig. 1*C* shows that FireCCISFD11 exceeded other BA products almost everywhere, and differences between the BA estimates were mostly dependent on BA patch size (Table 1). Small fires (<100 ha or roughly 4 MODIS 500-m pixels) accounted for 41.35% of overall BA in the FireCCISFD11 product but only 4.77% in MCD64A1C6 and 4.92% in the GFA. As a result, the FireCCISFD11 product estimated 15.61 times more BA in this fire-size class than the MCD64A1 product (2.02 versus 0.13 Mkm^2) and 16.24 times more than the GFA (0.12 Mkm^2). The difference in BA estimates between FireCCISFD11 and the other BA products increased with decreasing fire size. This was expected because smaller fires are less likely to be detected by coarse-resolution products. In fact, from the fires smaller than 25 ha (roughly 1 MODIS 500-m pixel) detected by the FireCCISFD11 product, only 2.09% were included in the MCD64A1C6 product and 2.23% in the GFA. For larger fires (>100 ha), the estimates derived from the coarse- and medium-resolution products were much closer: FireCCISFD11 had only 10.80% more BA in this size category than MCD64A1C6 and 19.25% more than GFA. These differences between the medium- and coarse-resolution sensors were related to a better characterization of large patches identified in both products, including both undetected pixels in the MODIS patches and over-detected pixels (unburned islands within burned patches) (27).

Small fires occurred throughout the study area, but their relative contribution to total BA was variable and often increased when total BA decreased (Fig. 2): near the coast of Liberia, Ivory Coast, Ghana, and Nigeria; in the western regions of Ethiopia, Mozambique, and Kenya; and in Zimbabwe and eastern South Africa. However, in some regions with high fire occurrence, the contribution of small fires to total BA was substantial as well, such as in Southern Zambia and Western Madagascar.

Seasonal Trends

Besides large differences in total BA, the temporal distribution of BA occurrence also differed between the FireCCISFD11 and

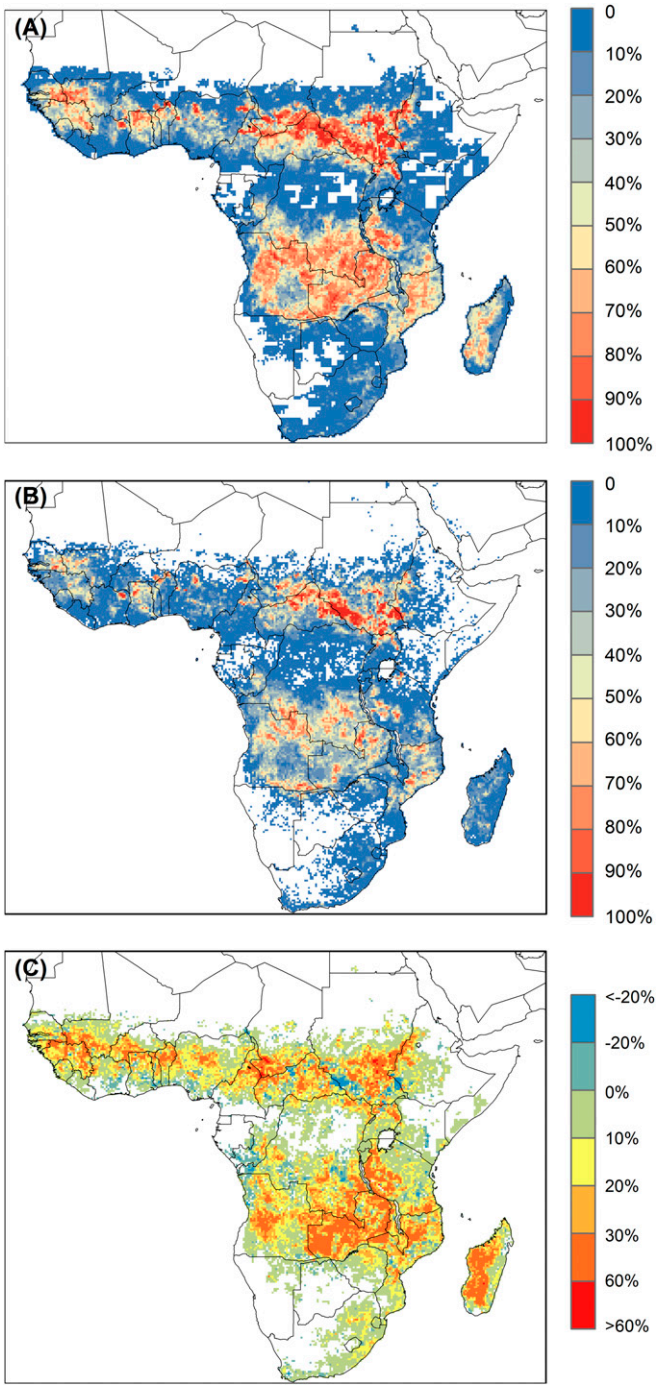

Fig. 1. Area burned in 2016, expressed as the fraction of each 0.25° grid cell according to FireCCISFD11 (*A*), GFED4s (*B*), and the difference of fractions between them (FireCCISFD11-GFED4s) (*C*). The rectangular blank grids in *A* correspond to S2 scenes where no active fires were detected by MODIS sensors in 2016. Therefore, no BA was mapped in those tiles.

Table 1. BA for 2016 clustered by fire size for FireCCISFD11, MCD64A1, and the GFA, the difference between the products, and the relative contribution of each fire-size class to the total BA estimated by the FireCCISFD11 product

Product	BA by fire size (km^2)			% BA in small fires (<100 ha)
	<100 ha	>100 ha	Total	
FireCCISFD11	2,024,070	2,871,045	4,895,115	41.35
MCD64A1	129,648	2,591,139	2,720,786	4.77
GFA	124,660	2,407,633	2,532,293	4.92

MCD64A1 BA products. According to the MODIS product, 80% of total BA in Northern Hemisphere Africa occurred during the 4 months of November through February, while 70% of BA in Southern Hemisphere Africa occurred during the 4 months of June through September. The FireCCISFD11 product identified a longer fire season, with 71% and 65% of the total BA occurring in those four peak months in the Northern and Southern Hemispheres, respectively (Fig. 3). This longer fire season is related to the improved detection of small fires, as they tend to have a larger share in fire activity outside the main fire season when more humid conditions may prevent fire propagation (Fig. 3). Undetected fires in global BA products thus prolong the fire season into the transitions between wet and dry seasons. This also implies a longer period of deteriorated air quality and may explain some of the long-standing and, until now, poorly explained mismatches between bottom-up and top-down emission estimates (particularly CO and aerosols) of the southern Africa fire season (28).

Variability in Relevance of Small Fires between Land Cover Types

Table 2 shows total BA categorized by fire size over different land cover classes (see *Materials and Methods*) for the FireCCISFD11 and MCD64A1C6 products. The savanna and grassland classes were responsible for most BA in both products (82.6% in FireCCISFD11 and 85.9% in MCD64A1). The differences between them were most important for fires smaller than 100 ha (Tables 2 and 3). This was partly due to the larger share of cropland fires detected by FireCCISFD11 (14.4% of BA in small fires versus 9.4% from the small fires detected by the MCD64A1 product). Agricultural fires are difficult to detect, as fire and harvest yield similar changes in reflectance (29). Even though the increase in BA was largest in croplands, its contribution to total BA was relatively modest (Tables 2 and 3) compared to the increases found in grasslands and savannas. This indicates that uncertainties related to the difficulties in detecting BA in agricultural zones only marginally impact our overall results.

Emissions Estimates

Fire carbon emission estimates are fraught with uncertainty. According to GFED4 (without small fires), 0.82 petagrams of carbon (PgC) was emitted from fires in Africa in 2016, whereas GFED4s estimated 1.09 PgC by incorporating small fires based on a statistical approach. Uncertainties in these estimates relate not only to the crude representation of small fires but also to the very coarse (0.25°) modeling framework in GFED4(s), limiting the usefulness of ground truthing with local studies. A recent study (30) used the GFED modeling framework and showed that modeling at 500-m resolution dramatically improved the agreement with ground-based studies regarding fuel consumption, the key parameter needed when translating BA to emissions. Without accounting for small fires, that study estimated emissions of 0.71 PgC in 2016. The lower estimate as compared to GFED4(s) was mostly related to lower fuel consumption, following from the improved model calibration to ground-based measurements at higher spatial resolution.

We used that modeling framework at 500 m (30) but replaced the MCD64A1 BA with the CCISFD11 BA aggregated to 500 m (see *Materials and Methods*) and estimated fire carbon emissions of 1.44 PgC (Fig. 4). This is about 31% higher than GFED4s and more than double (+101%) the estimates by Van Wees (referred to as MCD64A1 [500 m] emissions in Fig. 4). Given that this estimate is based on improved BA estimates and can mimic measured fuel consumption, the estimate is better constrained than previous numbers. The increase in emissions compared to GFED4s is substantial, exceeding average annual fire emissions of South America. This indicates that, when upscaled to the entire globe, the new FireCCISFD11 BA could lead to substantially higher fire emissions than currently estimated.

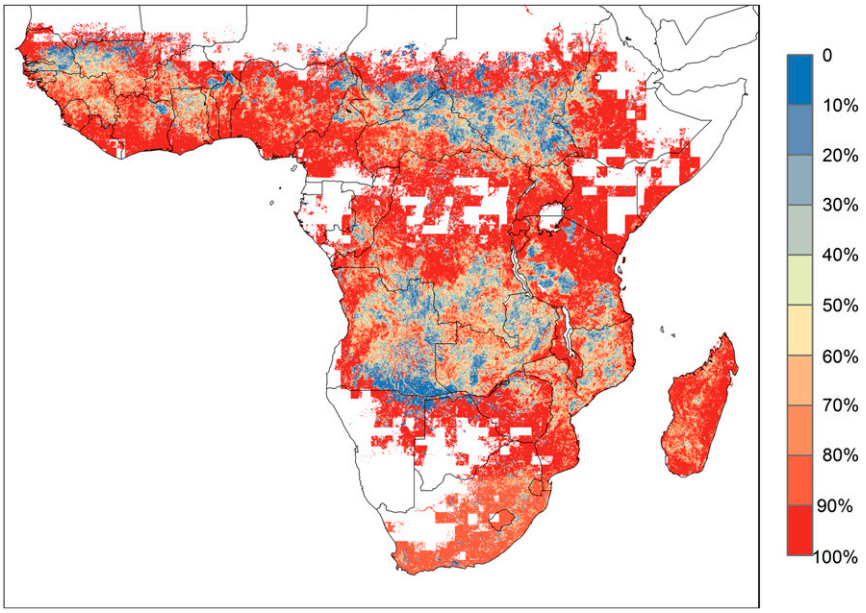

Fig. 2. Fraction of total BA stemming from fires smaller than 100 ha (plotted on a 0.05° grid) detected by the FireCCISFD11 product. The rectangular blank tiles correspond to MSI scenes where no active fires were detected and therefore do not include any BA.

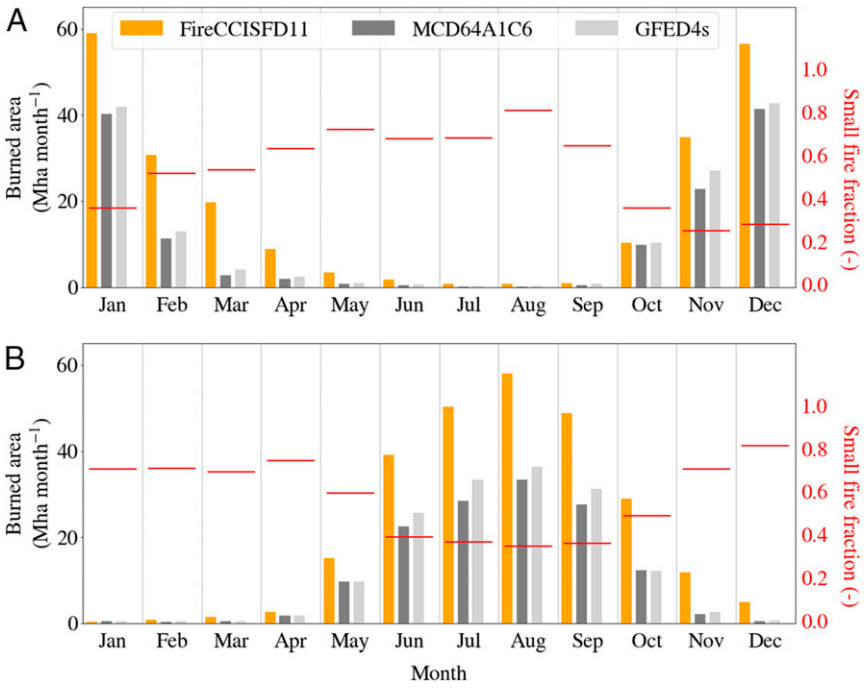

Fig. 3. Monthly BA estimates for FireCCISFD11, MCD64A1, and GFED4s for Northern Hemisphere (*A*) and Southern Hemisphere (*B*) Africa. The red line shows the proportion of fires <100 ha to total BA for the FireCCISFD11 product.

Implications for Our Understanding of Fire and Fire Emissions

This study compared medium- and coarse-resolution BA products at a continental scale, focusing on sub-Saharan Africa, which harbors the majority of global BA. We found that current estimates of global BA based on coarse-resolution sensors such as MODIS should be seen as very conservative (Table 1). A similar conclusion was gained by Laris (10) when comparing Landsat and MODIS BA products in a small savanna region of Mali and by some other authors in various ecosystems (11–15). Our BA estimates not only affect spatial assessments from previous estimations of total BA but also impact seasonal patterns of BA and fire emissions. The role of small fires has probably increased over past decades because of increases in population density and thus infrastructure and agriculture. Both lead to a more fragmented landscape that increasingly limits fire size. Since the resulting smaller fires are less likely to be detected by moderate-resolution BA products, they could offset part of the decline in BA observed in global products (18, 31). This hypothesis needs to be tested with future temporal analyses based on medium-resolution sensors.

Continental-scale spatial patterns of fire activity were fairly similar in the FireCCISFD11 and MCD64A1C6 BA datasets, but the increased amount of BA due to small fires varied regionally, with larger contributions in savanna and woody savanna areas as well as in agricultural areas. In addition, the greater proportion of BA observed during the transitions between wet and dry seasons in the FireCCISFD11 product suggests that fire seasons are longer than formerly thought, at least based on our analysis of the year 2016. The relative prevalence of small fires outside the regular fire season may be related to anthropogenic influences on fire regimes, as human fire management tends to concentrate on periods with higher rainfall rates to inhibit large fires later in the season when fuels are drier and fires burn more intensively (32, 33). This extended fire season may help explain why measurements of atmospheric carbon monoxide or aerosol concentrations suggest that fire seasons extend beyond the period suggested by coarse-resolution observations of BA (28, 34). The extension of the fire season lengthens the time of enhanced aerosol concentrations into the rainy season with potentially important impacts on cloud dynamics and radiative forcing. However, our most important finding is the systemic and large increase in BA with implications for atmospheric concentrations of trace gases and aerosols, ecology, and human exposure to deteriorated air quality.

Materials and Methods

The FireCCISFD11 product was generated from Sentinel-2 MSI data at 20-m resolution in combination with active fire observation from MODIS at 1-km resolution [MCD14ML (35)]. The algorithm used a multitemporal approach to classify BA using two consecutive acquisitions (21), extending the time span up to four previous acquisitions in cloudy regions. The MSI images were

Table 2. Total BA due to fires smaller than 100 ha separated by land cover type for FireCCISFD11 and MCD64A1

BA product	Croplands	Grasslands	Savanna	Forests	All
FireCCISFD11 (km^2)	291,614	751,834	918,108	60,865	2,022,421
MCD64A1 (km^2)	12,196	47,303	63,633	5,993	129,126
FireCCISFD11/MCD64A1	23.91	15.89	14.43	10.16	15.66
% of FireCCISFD11	14.42%	37.17%	45.40%	3.01%	100%

Relative differences and total percentage for each size class are shown.

Table 3. Total BA due to fires larger than 100 ha separated by fire land cover type for FireCCISFD11 and MCD64A1

BA product	Croplands	Grasslands	Savanna	Forest	All covers
FireCCISFD11 (km^2)	211,594	1,251,064	1,351,521	55,933	2,870,113
MCD64A1 (km^2)	173,911	1,136,470	1,233,667	45,231	2,589,280
FireCCISFD11/MCD64A1	1.22	1.10	1.10	1.24	1.11
% of FireCCISFD11	7.37%	43.59%	47.09%	1.95%	100%

Relative differences and total percentage for each size class are shown.

atmospherically corrected using the Sen2cor module (36), and unburnable areas were masked using the Scene Classification map, which contains clouds and cloud shadows, among others. The BA algorithm used the Near Infrared, Normalized Burned Ratio 2, and Mid-Infrared Burn Index to perform an initial classification of burned pixels using fixed thresholds. This classification was overlaid with MODIS active fires (MCD14ML) in order to localize pixels with a high burn probability as a way to compute regional thresholds for producing the final BA classification using a two-stage procedure (first detecting high burned probability seeds and then extending the burned regions in lower burned probability neighborhood). The dataset includes the date of detection, the burn probability, and the land cover affected by the fire.

The MCD64A1C6 (Collection 6 of the MCD64A1 product) BA product was derived from images acquired by the MODIS sensors onboard the Terra and Aqua satellites. It has a 500-m spatial resolution and provides daily global fire information based on level 2 surface-reflectance imagery. The BA algorithm included different phases. First, time series were extracted based on cloud-free pixels. Then, a burn-sensitive index was computed based on bands 5 and 7 of the MODIS sensor (in the short-wave infrared region) to calculate composites. This information was combined with active fire observations to characterize prefire and postfire conditions, deriving the fire-related changes. The results of this phase were used to estimate thresholds to carry out the final BA assessment (22).

The MCD64A1 BA datasets have been traditionally used as input for GFED, which is one of the most widely used fire emission datasets in atmospheric and biogeochemical models (37, 38). In this study, we used the latest version of GFED, named GFED4s (23). GFED4s uses BA from a previous MCD64A1 dataset, Collection 5.1, but aimed to account for the effects of small fires using active fire observations from MODIS (18). The contribution of small fires was estimated using a statistical approach based on overlaying active fire detections and mapped BA. Even though active fire products have an even lower spatial resolution than the MCD64A1 products (1 km versus 500 m), the thermal contrast between hot spots and background surfaces is very large in the mid infrared band, allowing detection of active fires far smaller than the pixel resolution. Based on this, the contribution of small fires was computed using the proportion of active fires that fell inside and outside of the burned perimeters in combination with ancillary data to assess how much BA an active fire represents. Using this BA dataset, GFED4s emissions were also calculated at 0.25° grid level using various additional satellite datasets to simulate the carbon cycle and fuel consumption (23).

The FireCCISFD11 product was validated using systematic sampling of 52 Sentinel image pairs (100 × 100 km), in which fire perimeters were obtained from an independent, multitemporal classification approach (39) and then visually inspected. The validation was performed by land cover types, and it was based on the Sentinel-2 land cover map generated by the LC-CCI project (http://www.esa-landcover-cci.org/) (Table 4). Error matrices estimated a commission error of 8.1% and an omission error of 24.5% with a Dice Coefficient (DC) of 0.83. The main commission errors were found in sparse vegetation, urban areas, and in the borders of clouds/cloud shadows, which were undetected by the Sentinel Scene Classification Mask. Similar accuracy values were found for the most relevant land cover types for this study

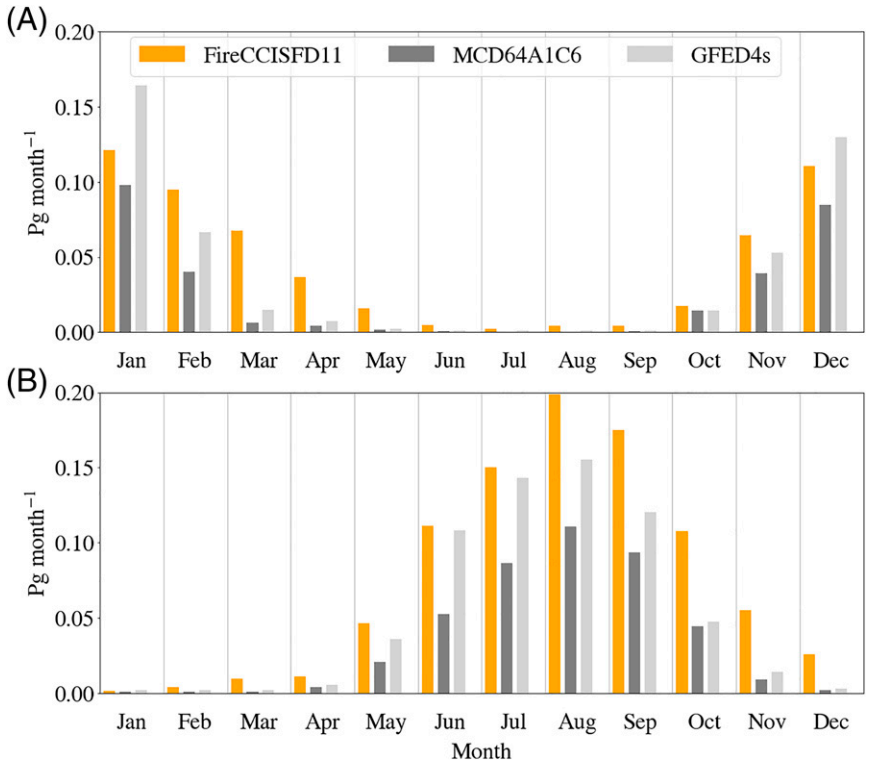

Fig. 4. Monthly carbon emission estimates based on FireCCISFD11 and MCD64A1 BA using the 500-m model by Van Wees et al. (28) and emissions from GFED4s (0.25°) for Northern Hemisphere (*A*) and Southern Hemisphere (*B*) Africa.

Table 4. Accuracy metrics for the S-2 validation dataset

	OE	CE	Relb	DC
Forest	25.4	7.7	−0.236	82.5
Agriculture	18.5	11.8	−0.083	84.7
Scrubland	22.4	6.4	−0.206	84.9
Grassland	37.3	5.6	−0.506	75.4
Sparse vegetation	95.5	99.2	0.830	1.3
Bare area	33.6	13.8	−0.299	75.0
Wetland	29.1	11.1	−0.254	78.9
Water	14.7	7.0	−0.090	89.0
Settlement	33.5	48.3	0.224	58.2
All covers	24.5	8.1	−0.218	82.9

Omission errors (OE), commission errors (CE), relative bias (Relb), and dice coefficient (DC) are shown.

(croplands, shrublands, and forest) with a DC value close to 0.82. Sparse vegetation, wetlands, and settlements had a very low proportion of the sample areas (2.5%). Average errors of the FireCCISFD11 product were significantly lower than those of existing global products (15, 17, 21). For instance, a recent validation exercise of the MCD64A1 BA product, based on a stratified random sampling strategy and using Landsat-8 images as reference sites, estimated a global commission error of 40.2% and a global omission error of 72.6% (15), confirming the tendency of this global BA product to underestimate BA.

The generation of burn patches in both the FireCCISFD11 and MCD64A1 products was based on a flood-fill algorithm. Individual patches were identified, assigning a unique value to pixels that had less than 10 d of temporal difference (the Sentinel-2 temporal gap) and were connected by a 3×3 pixel moving window. After that, the area for each individual fire path was computed by transforming from geographical to planar coordinates. This process was applied for each month and tile. When pixels from the first image of the temporal comparison (tn-1) were unobserved, the comparison was extended to the second or third prefire image (tn-2 or tn-3). The GFA (24) developed a more sophisticated method to obtain burn patches based on fire propagation patterns. The input dataset for the GFA also was the MCD64A1C6 product, so we were able to compare the impact of using two different methods to obtain fire patches on the total fire-size distribution of the continent.

To better characterize the spatial distribution of BA, two auxiliary datasets were used to construct a land cover map: the land cover dataset developed using Sentinel 2 images (26, 40) that comprises 10 classes following the recommendation of the Global Terrestrial Observing System and the Vegetation Continuous Fields (41) that shows the percentage of tree or vegetation cover as a quantitative variable. The land cover map had four classes: 1) croplands extracted from the Sentinel-2 LC map, 2) grasslands that grouped those pixels not classified as cropland and that had less than 10% of tree cover, 3) savanna and woody savannas with a tree cover between 10 and 50%, and 4) forest, which has more than 50% of tree cover.

For the MCD64A1 product, we resampled both the BA and the land cover to a common pixel size of 100 m to reduce errors related to border effects and to facilitate the processing. The resampling was done using the most dominant categories in both the BA and the land cover products. Using cross-tabulation analysis, each fire patch was labeled with the fire size and the number of pixels of each land cover class. From this dataset, the burned proportion and total BA of each land cover class were computed.

The 500-m resolution fire emission model developed by Van Wees and Van der Werf (30) is a simplified version of the GFED modeling framework based on BA from the MCD64A1C6 dataset and other MODIS products for the modeling of aboveground biomass. Mechanisms such as belowground carbon dynamics, herbivory, and mechanisms specific to deforestation were not included, maintaining only the most important functionality for fire emission estimation. The 500-m model was tuned using satellite-based data on aboveground biomass (42) and field measurements on fuel load and consumption (43), also used for the validation of GFED4(s). The substantially higher spatial resolution of 500 m (versus 0.25° in GFED) led to lower fuel consumption values, mostly as a result of reduced representation errors in the comparison of the model to field measurements. This resulted in 24% lower fire emissions (0.68 $PgC \cdot yr^{-1}$) for the 2002 to 2017 period in sub-Saharan Africa as compared to GFED4 (without small fires). This model was applied here to calculate emissions based on FireCCISFD11 and MCD64A1 BA at 500-m resolution. Emissions based on FireCCISFD11 BA were calculated by replacing the MODIS BA data with the FireCCISFD11 BA aggregated to 500 m, and results were compared with the GFED4s emission product.

Data Availability. BA data have been deposited in FireCCISFD11 (https://dx.doi.org/10.5285/065f6040ef08485db989cbd89d536167) (44).

ACKNOWLEDGMENTS. We would like to thank Niels Andela for his recommendations on characterizing fire size. This research has been financed by the European Space Agency through the FireCCI project (Contract 4000126706/19/I-NB). R.R. was funded by the University of Alcalá's Predoctoral Fellowship Program. G.R.v.d.W. and D.v.W. received funding from the Netherlands Organisation of Scientific Research.

1. S. Kloster, G. Lasslop, Historical and future fire occurrence (1850 to 2100) simulated in CMIP5 Earth System Models. *Global Planet. Change* **150**, 58–69 (2017).
2. D. M. Bowman *et al*., Human exposure and sensitivity to globally extreme wildfire events. *Nat. Ecol. Evol.* **1**, 0058 (2017).
3. C. I. Roos *et al*., Living on a flammable planet: Interdisciplinary, cross-scalar and varied cultural lessons, prospects and challenges. *Philos. Trans. R Soc. Lond. B Biol. Sci.* **371**, 20150469 (2016).
4. A. Benali *et al*., Bimodal fire regimes unveil a global-scale anthropogenic fingerprint. *Glob. Ecol. Biogeogr.* **26**, 799–811 (2017).
5. D. Morton *et al*., Agricultural intensification increases deforestation fire activity in Amazonia. *Glob. Change Biol.* **14**, 2262–2275 (2008).
6. D. Ward *et al*., The changing radiative forcing of fires: Global model estimates for past, present and future. *Atmos. Chem. Phys.* **12**, 10857–10886 (2012).
7. D. Chen, T. V. Loboda, T. He, Y. Zhang, S. Liang, Strong cooling induced by stand-replacing fires through albedo in Siberian larch forests. *Sci. Rep.* **8**, 4821 (2018).
8. G. López-Saldaña, I. Bistinas, J. Pereira, Global analysis of radiative forcing from fire-induced shortwave albedo change. *Biogeosciences* **12**, 557–565 (2015).
9. E. Chuvieco *et al*., Historical background and current developments for mapping burned area from satellite Earth observation. *Remote Sens. Environ.* **225**, 45–64 (2019).
10. P. S. Laris, Spatiotemporal problems with detecting and mapping mosaic fire regimes with coarse-resolution satellite data in savanna environments. *RSE* **99**, 412–424 (2005).
11. J. A. Anaya, E. Chuvieco, Accuracy assessment of burned area products in the Orinoco basin. *PERS* **78**, 53–60 (2012).
12. S. Mangeon, R. Field, M. Fromm, C. McHugh, A. Voulgarakis, Satellite versus ground-based estimates of burned area: A comparison between MODIS based burned area and fire agency reports over North America in 2007. *The Anthropocene Review* **3**, 76–92 (2016).
13. D. P. Roy, L. Boschetti, Southern Africa validation of the MODIS, L3JRC, and GlobCarbon burned-area products. *Ieee T Geosci Remote* **47**, 1032–1044 (2009).
14. E. Chuvieco *et al*., Global burned-land estimation in Latin America using MODIS composite data. *Ecol. Appl.* **18**, 64–79 (2008).
15. L. Boschetti *et al*., Global validation of the collection 6 MODIS burned area product. *Remote Sens. Environ.* **235**, 111490 (2019).
16. E. Chuvieco *et al*., Generation and analysis of a new global burned area product based on MODIS 250 m reflectance bands and thermal anomalies. *Earth Syst. Sci. Data* **10**, 2015–2031 (2018).
17. J. Lizundia-Loiola, G. Otón, R. Ramo, E. Chuvieco, A spatio-temporal active-fire clustering approach for global burned area mapping at 250 m from MODIS data. *Remote Sens. Environ.* **236**, 111493 (2020).
18. J. Randerson, Y. Chen, G. Werf, B. Rogers, D. Morton, Global burned area and biomass burning emissions from small fires. *J. Geophys. Res. Biogeosci.* **117**, G04012 (2012).
19. T. J. Hawbaker *et al*., Mapping burned areas using dense time-series of Landsat data. *Remote Sens. Environ.* **198**, 504–522 (2017).
20. T. Long *et al*., 30 m resolution global annual burned area mapping based on landsat images and Google Earth engine. *Remote Sens.* **11**, 489 (2019).
21. E. Roteta, A. Bastarrika, M. Padilla, T. Storm, E. Chuvieco, Development of a Sentinel-2 burned area algorithm: Generation of a small fire database for sub-Saharan Africa. *Remote Sens. Environ.* **222**, 1–17 (2019).
22. L. Giglio, L. Boschetti, D. P. Roy, M. L. Humber, C. O. Justice, The Collection 6 MODIS burned area mapping algorithm and product. *Remote Sens. Environ.* **217**, 72–85 (2018).
23. G. R. van der Werf *et al*., Global fire emissions estimates during 1997–2016. *Earth Syst. Sci. Data* **9**, 697 (2017).
24. N. Andela *et al*., The Global Fire Atlas of individual fire size, duration, speed and direction. *Earth Syst. Sci. Data* **11**, 529–552 (2019).
25. F. Mouillot *et al*., Ten years of global burned area products from spaceborne remote sensing—A review: Analysis of user needs and recommendations for future developments. *Int. J. Appl. Earth Obs. Geoinf.* **26**, 64–79 (2014).
26. P. Defourny, M. Santoro, G. Kirches, J. Wevers, M. Boettcher, Land Cover CCI Product User Guide Version 2. http://maps.elie.ucl.ac.be/CCI/viewer/download/ESACCI-LC-Ph2-PUGv2_2.0.pdf. Accessed 9 February 2021.
27. E. Roteta, A. Bastarrika, T. Storm, E. Chuvieco, Development of a Sentinel-2 burned area algorithm: generation of a small fire database for northern hemisphere tropical Africa. *Remote Sens. Environ.* **222**, 1–17 (2019).

28. B. Zheng, F. Chevallier, P. Ciais, Y. Yin, Y. Wang, On the role of the flaming to smoldering transition in the seasonal cycle of African fire emissions. *Geophys. Res. Lett.* **45**, 11,998–12,007 (2018).
29. J. V. Hall, T. V. Loboda, L. Giglio, G. W. McCarty, A MODIS-based burned area assessment for Russian croplands: Mapping requirements and challenges. *RSE* **184**, 506–521 (2016).
30. D. Van Wees, G. R. Van Der Werf, Modelling biomass burning emissions and the effect of spatial resolution: A case study for Africa based on the global fire emissions database (GFED). *Geosci. Model Dev.* **12**, 4681–4703 (2019).
31. N. Andela *et al*., A human-driven decline in global burned area. *Science* **356**, 1356–1362 (2017).
32. P. Laris, Burning the seasonal mosaic: Preventative burning strategies in the wooded savanna of southern Mali. *Hum. Ecol.* **30**, 155–186 (2002).
33. J. Russell-Smith, P. G. Ryan, R. Durieu, A LANDSAT MSS-Derived fire history of kakadu national park, monsoonal northern australial, 1980-94: Seasonal extent, frequency and patchiness. *J. Appl. Ecol.* **34**, 748–766 (1997).
34. G. R. van der Werf *et al*., Interannual variability in global biomass burning emissions from 1997 to 2004. *Atmos. Chem. Phys.* **6**, 3423–3441 (2006).
35. L. Giglio, W. Schroeder, C. O. Justice, The collection 6 MODIS active fire detection algorithm and fire products. *Remote Sens. Environ.* **178**, 31–41 (2016).
36. J. Louis *et al*., Sentinel-2 Sen2Cor: L2A processor for users. https://elib.dlr.de/107381/1/LPS2016_sm10_3louis.pdf. Accessed 9 February 2021.
37. S. Schwietzke *et al*., Upward revision of global fossil fuel methane emissions based on isotope database. *Nature* **538**, 88–91 (2016).
38. B. Aouizerats, G. R. Van Der Werf, R. Balasubramanian, R. Betha, Importance of transboundary transport of biomass burning emissions to regional air quality in Southeast Asia during a high fire event. *Atmos. Chem. Phys.* **15**, 363–373 (2015).
39. A. Bastarrika *et al*., BAMS: A tool for supervised burned area mapping using landsat data. *Remote Sens.* **6**, 12360–12380 (2014).
40. Y. Xu *et al*., Comparisons of three recent moderate resolution African land cover datasets: CGLS-LC100, ESA-S2-LC20, and FROM-GLC-Africa30. *Int. J. Remote Sens.* **40**, 6185–6202 (2019).
41. M. Hansen *et al*., Global percent tree cover at a spatial resolution of 500 meters: First results of the MODIS vegetation continuous fields algorithm. *Earth Interact.* **7**, 1–15 (2003).
42. V. Avitabile *et al*., An integrated pan-tropical biomass map using multiple reference datasets. *Glob. Change Biol.* **22**, 1406–1420 (2016).
43. T. T. van Leeuwen *et al*., Biomass burning fuel consumption rates: A field measurement database. *Biogeosciences* **11**, 7305–7329 (2014).
44. E. Chuvieco *et al*., ESA Fire Climate Change Initiative (Fire_cci): Small Fire Dataset (SFD) Burned Area pixel product for Sub-Saharan Africa, version 1.1. Centre for Environmental Data Analysis Archive. http://dx.doi.org/10.5285/065f6040ef08485db989cbd89d536167. Deposited 12 October 2018.